Available online at www.sciencedirect.com
ScienceDirect
Trans. Nonferrous Met. Soc. China 32(2022) 2125−2137
Transactions of Nonferrous Metals Society of China
www.tnmsc.cn

Non-isothermal aging behavior of in-situ AA2024−Al_3NiCu composite

Ramezanali FARAJOLLAHI, Hamed JAMSHIDI AVAL, Roohollah JAMAATI

Department of Materials Engineering, Babol Noshirvani University of Technology, Shariati Avenue, Babol 47148-71167, Iran

Received 3 August 2021; accepted 9 March 2022

Abstract: The effect of non-isothermal aging treatment on microstructure and mechanical properties of in-situ AA2024−Al_3NiCu composite fabricated by the stir casting process was examined. The Al_3NiCu intermetallic was created by adding 3 wt.% nickel powder during stir casting and homogenization treatment at 500 °C for 24 h after casting. The microstructural results obtained using optical and scanning electron microscope indicate that, after non-isothermal aging treatment, the *S*-Al_2CuMg precipitates become finer, forming a poor zone of this precipitate in the area between the dendrites. Also, adding nickel during stir casting reduces the precipitation rate and the contribution of *S*-Al_2CuMg precipitates in strengthening composite during non-isothermal aging. The maximum hardness, ultimate tensile strength, and toughness achieved in the 3 wt.% nickel-containing sample after non-isothermal aging at 250 °C are (121.30±4.21) HV, (221.67±8.31) MPa, and (1.67±0.08) MJ/m^3, respectively. The maximum hardness and ultimate tensile strength of AA2024−Al_3NiCu composite are decreased by 6% and 4%, respectively, compared to those of nickel-free AA2024 aluminum alloy.

Key words: AA2024 aluminum matrix composite; stir casting method; non-isothermal aging treatment; Al_3NiCu reinforcement

1 Introduction

Our growing needs and the depleting sources of natural raw materials such as metals have compelled us to use modern technology to produce materials that satisfy most of our needs with minimum cost. Metal matrix composites (MMCs) are among these materials. In these composites, a metal matrix such as titanium, aluminum, and magnesium is reinforced using ceramic or metal reinforcements [1−4]. The MMCs can show high strength and modulus of elasticity, high coefficient of thermal expansion, and heat resistance based on the nature and volume percentage of reinforcements and matrix, and the type of heat treatment and fabrication processes involved [5,6]. Compared to conventional metals and alloys, MMCs, as a group of advanced materials, have several advantages, such as weight savings due to the high specific strength, better dimensional stability due to lower thermal expansion, as well as creep, high cyclic fatigue and wear resistance. Also, MMCs have many applications in the transportation industry, marine equipment, and electrical equipment industry [7].

Among the metals used as matrix in MMCs, aluminum has attractive and unique properties, such as being lightweight, available, and low-price, allowing it to be widely used as a matrix in the fabrication of MMCs. Previous research indicates that among various MMCs fabrication methods, solidification-based processes such as stir casting have tremendous potential for the cost-effective mass production of engineering parts [8−10]. One of the problems of adding reinforcing particles in

Corresponding author: Hamed JAMSHIDI AVAL, Tel: +98-11-35501808, Fax: +98-11-35501800, E-mail: h.jamshidi@nit.ac.ir
DOI: 10.1016/S1003-6326(22)65935-1

melting methods is the lack of complete wettability of the reinforcing agents by the metal melt and the lack of high joint strength. The use of metal particles with limited solubility in aluminum can potentially solve the problem of the wettability of reinforcing particles in the aluminum melt. When a chemical reaction occurs, the reinforcing particles form a strong metallurgical bond with the aluminum matrix. Nickel is used to reinforce aluminum matrix composites (AMCs) [11,12]. Compared to ceramics, nickel has better wettability with molten aluminum, making it a good candidate as a reinforcing phase in the manufacture of AMCs to improve different properties, such as strength, hardness, and toughness due to the formation of nickel-aluminide intermetallics [13].

Many researchers have extensively studied the fabrication of AMCs reinforced with nickel-aluminide using casting methods. ARUL [14] noted that the improvement in microhardness and wear resistance of nickel-reinforced AA7075 matrix composites fabricated using stir casting process could be related to Al_3Ni intermetallic compounds (IMCs) in the matrix. VISHWANATHA et al [15] investigated the effect of T6 heat treatment on the corrosion behavior of nickel powder-reinforced AA6061 matrix composite fabricated by the stir casting process. They found that corrosion current increased and polarization resistance decreased in both as-cast and aged conditions with increasing nickel addition. However, T6 heat-treated samples showed weaker corrosion resistance compared to as-cast composites. ABUTHAKIR et al [16] studied the corrosion resistance of the AA6061 matrix composite reinforced with nickel particles. They found that the corrosion current increased with increasing atomic percentage of nickel in the nickel-aluminide intermetallic compounds. In addition, they reported that the composite containing Al_4Ni intermetallic compounds showed higher corrosion resistance than other composites. RAMESH et al [17] fabricated an AA1100−Al_3Ni in-situ composite using squeeze and stir casting methods. They predicted that increasing the amount of Al_3Ni would improve the mechanical and wear resistance of the composite. Furthermore, it was reported that the squeeze-cast composites might be superior to the stir cast ones. MATSUMURO and KITSUDO [18] investigated the effect of adding nickel to an aluminum melt during the stir casting process and the formation of an in situ Al_3Ni reinforced composite. They reported that Al_3Ni reinforcement amounts decreased with decreasing stirring temperature and stirring time.

An important point to note is the effect of the reinforcements on the precipitation hardening behavior of aluminum alloy used as the matrix. One of the purposes of using precipitation-hardenable aluminum alloy as the matrix of composite is to take advantage of the precipitates strengthening mechanisms on the mechanical properties of the final product. The use of reinforcing particles with high or even partial solubility in the matrix can affect the precipitation behavior of the matrix alloy. In this study, nickel was added to molten AA2024 aluminum alloy during stir casting to study the effect of nickel on the non-isothermal aging behavior of AA2024 matrix composite reinforced with nickel-rich compounds.

2 Experimental

AA2024 aluminum alloy with a chemical composition of 0.14% Si, 0.26% Fe, 4.14% Cu, 0.49% Mn, 1.45% Mg, and Al balance (all in wt.%) and nickel powder with a size of 20−70 μm were used as the matrix and reinforcement in the fabrication of AMC in the stir casting process (for a schematic of the process, see Fig. 1). Argon gas was used to create a protective atmosphere in stirring the melt and as a carrier gas for nickel powder. The casting process began in the preheated graphite crucible. Hexachloroethane (C_2Cl_6) tablets were used for degassing in the melt. The stirrer was then introduced into the melt, and the stirring operation was started by an electric motor equipped with a speed adjustment system. After the nickel powder

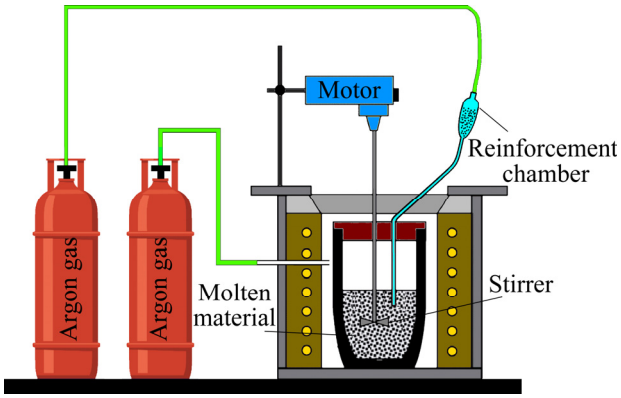

Fig. 1 Schematic view of stir casting procedure

injection was complete, stirring was continued for 2 min. Finally, the crucible was taken out of the furnace, and a long cylindrical mold with a diameter of 22 mm and a length of 200 mm was used to discharge the molten component. According to a previous study [19], the optimal nickel mass fraction, stirring speed, stirring time, and stirring temperature were 3%, 300 r/min, 20 min, and 750 °C, respectively. Therefore, this study used the parameters mentioned above for AMC fabrication.

After casting and cooling the cast parts, metallographic samples and tensile tests were prepared from the center of rods. In order to investigate the effect of non-isothermal aging heat treatment, first, homogenized samples were solutionized at 505 °C for 140 min and, after quenching in the water, subjected to non-isothermal aging with a heating rate of 10 °C/min. The homogenization heat treatment was performed at 500 °C for 24 h on all samples. The homogenizing treatment temperature and time were chosen according to a preliminary study by authors and the best temperature−time reported in Ref. [20] to achieve maximum mechanical properties. For the microstructural examination, grinding was performed with sandpaper, then the samples were polished using alumina suspension and finally etched with Keller etchant (2.5 mL nitric acid, 1.5 mL hydrochloric acid, and 1 mL hydrofluoric acid). Tensile test was performed according to ASTM E8M standard using tensile samples with a gauge length of 24 mm and a diameter of 6 mm. The tensile test was performed using a SANTAM-STM250 testing machine at a constant crosshead speed of 1 mm/min and three repeating times to determine the mechanical properties. The toughness was calculated using the area underneath the stress−strain curve. The macro Vickers hardness test was performed using the KOOPA-UV1 universal hardness tester following the ASTM E92 standard at a load of 10 kg, a duration of 10 s, and averaging at least 20 indentations. In order to more accurately measure the diameter of indentation left in the test material, the load of 10 kg was used. Differential scanning calorimetry (DSC) test was performed using DSC 204 Phoenix for the precipitation behavior analysis of the composite samples. For this purpose, the prepared sample with the dimensions of 2.5 mm × 2.5 mm × 1 mm was initially exposed for 2 h at temperature of 515 °C. It was then quenched with water and immediately placed in the DSC machine and heated at a rate of 10 °C/min. According to Archimedes' principle [21] and the mixture rule, the porosity of samples (P) was calculated as follows:

$$P=(1-(\rho_s/\rho_{th}))\times 100\% \quad (1)$$

where ρ_s and ρ_{th} denote the composite density and the theoretical value of the porosity-free density, respectively.

3 Results and discussion

3.1 Microstructure evolution

Figure 2 shows the sample's microstructure with and without nickel in different magnifications. As shown, porosity is visible in both microstructures regardless of the presence or absence of nickel in the composite. The porosity in the microstructure of these two samples can occur due to shrinkage or gas trapping. The porosity in the nickel-containing and nickel-free samples is (3.2±0.9)% and (2.1±1.1)%, respectively. The higher porosity percentage in the nickel-containing sample is probably due to the trapping of part of the carrier gas in the melt during the addition of nickel powder. Agglomerated nickel-rich particles can also provide places for porosity formation and trapping gas. Irrespective of the nickel-rich intermetallic compounds formed by adding nickel to the nickel-containing sample, which is mainly gray in microstructure, the intermetallic compounds, precipitates, and eutectic structure are formed in both nickel-containing and nickel-free samples. However, it should be noted that adding nickel decreases the amount of eutectic structure in the microstructure. Another distinguishing feature of the microstructure in these two samples is the formation of dark blade structures in the microstructure of the nickel-containing sample, visible in large quantities in the microstructure. In addition to the formation of fine black precipitates in the inter-dendritic zone in both samples, it is observed that the grain size of aluminum in two samples containing nickel and without nickel are (28.4±4.6) and (29.7±5.8) μm, respectively. Although the difference between the grain sizes of the two samples is not very noticeable, the smaller grain size in nickel-containing samples indicates that the formation of nickel-rich compounds acts as

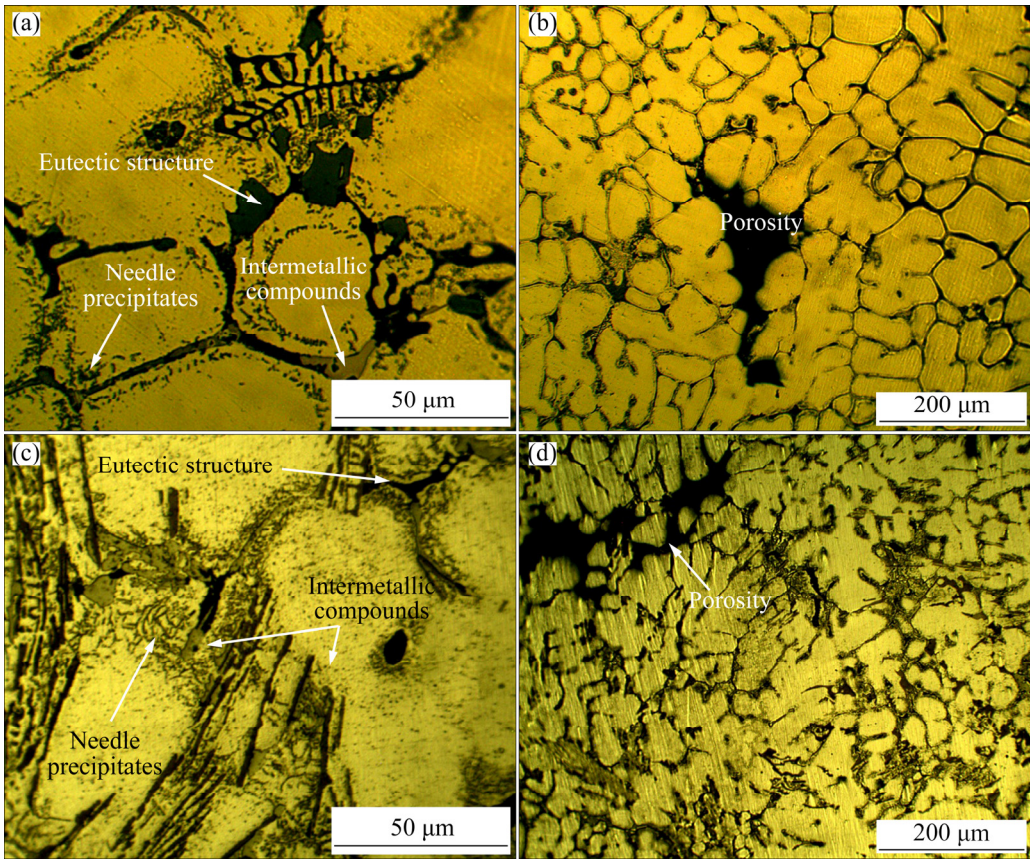

Fig. 2 Optical microscopy images of nickel-free (a, b) and nickel-containing (c, d) samples at different magnifications

nucleation sites for aluminum grain and prevents grain growth and the formation of coarse-grained microstructure in the nickel-containing sample.

Figure 3 shows the microstructure of the nickel-containing and nickel-free samples with different time of non-isothermal heat treatment. After homogenization, the amount of eutectic structure decreases in both samples, and the morphology of intermetallic compounds remains unchanged, displaying some growth. As the aging temperature increases, it is observed that the number of black precipitates formed in the microstructure increases; these precipitates are mainly formed inside the grains, forming a precipitate-free zone at the interdendritic zone. However, it should be noted that with the addition of nickel in AA2024 aluminum alloy, the number of black precipitates formed in the microstructure decreases.

In order to investigate the nature of precipitates and intermetallic compounds formed in the two samples, the SEM results related to the microstructure of different samples are shown in Fig. 4. The EDS results of various compounds and precipitates are presented in Figs. 5, 6 and Table 1. For both samples in the as-cast state, *S*-Al_2CuMg, Al_7Cu_2Fe, and Al(Cu,Mn,Fe,Si) precipitates and intermetallic compounds are observed. Also, in the nickel-containing sample, the Al_3NiCu intermetallic compounds are visible. After solid solution and aging treatment, it is observed that in both samples, regardless of the presence or absence of nickel in the microstructure, the *S*-Al_2CuMg precipitates are formed in the interdendritic zone.

It should be noted that the size of *S*-Al_2CuMg precipitates decreases with the addition of nickel in the microstructure. As shown in Fig. 4, after aging treatment, the *S*-Al_2CuMg precipitates become finer, and a poor zone of this precipitate is formed in the area between the dendrites. This phenomenon can be attributed to the diffusion of copper during heat treatment to nickel or iron-rich compounds, which will reduce the amount of soluble copper in the aluminum matrix. According to the EDS results as well as the XRD results of as-cast samples reported in Ref. [19], the nature of the precipitates formed in the microstructure does not change. Based on Refs. [22−24], the ratio of copper to magnesium is

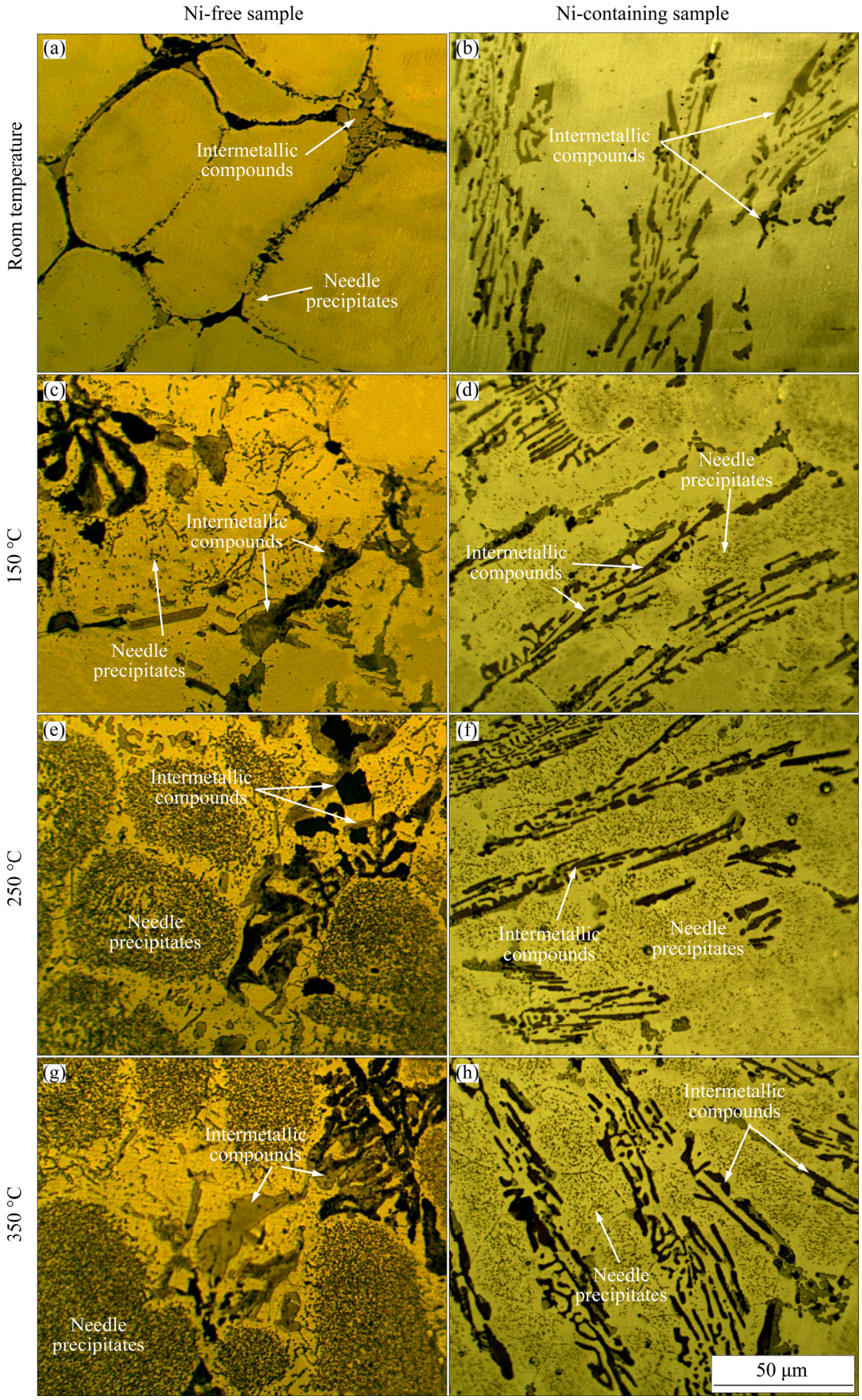

Fig. 3 Optical microscopy images of nickel-free and nickel-containing samples at different non-isothermal aging temperatures

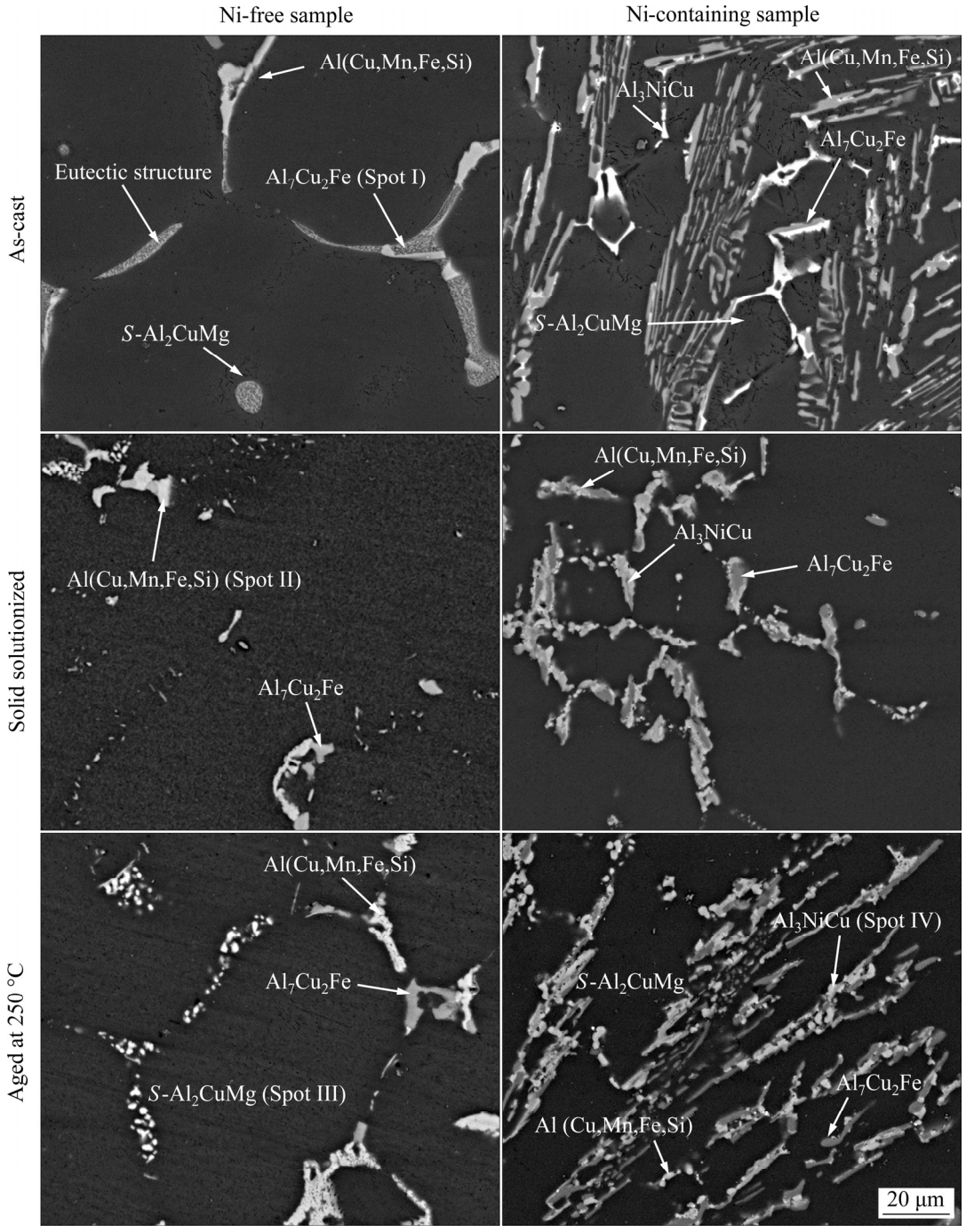

Fig. 4 SEM images of nickel-free and nickel-containing samples under different conditions

the determining factor in the type of precipitates formed in the microstructure. It has been reported that for ratios greater than 8, the Al−Cu−Mg alloys are strengthened by precipitation of the θ-Al_2Cu phase. However, for ratios between 4 and 8, θ-Al_2Cu and S-Al_2CuMg constitute the main strengthening phases. The S-Al_2CuMg is the most effective strengthening phase in Al−Cu−Mg systems with a low ratio (1.5−4). According to EDS analysis after solid solution treatment, the amounts of soluble copper in the aluminum matrix in nickel-free and nickel-containing samples are 2.8 wt.% and 3.4 wt.%, respectively. Also, the amounts of soluble magnesium in the aluminum matrix are 1.3 wt.% and 1.4 wt.%, respectively. The reported values indicate that the ratio of copper to magnesium in nickel-containing and nickel-free samples are 2.1 and 2.4, respectively. According to Ref. [25], based on the ratio of copper to magnesium in these two samples, the precipitates

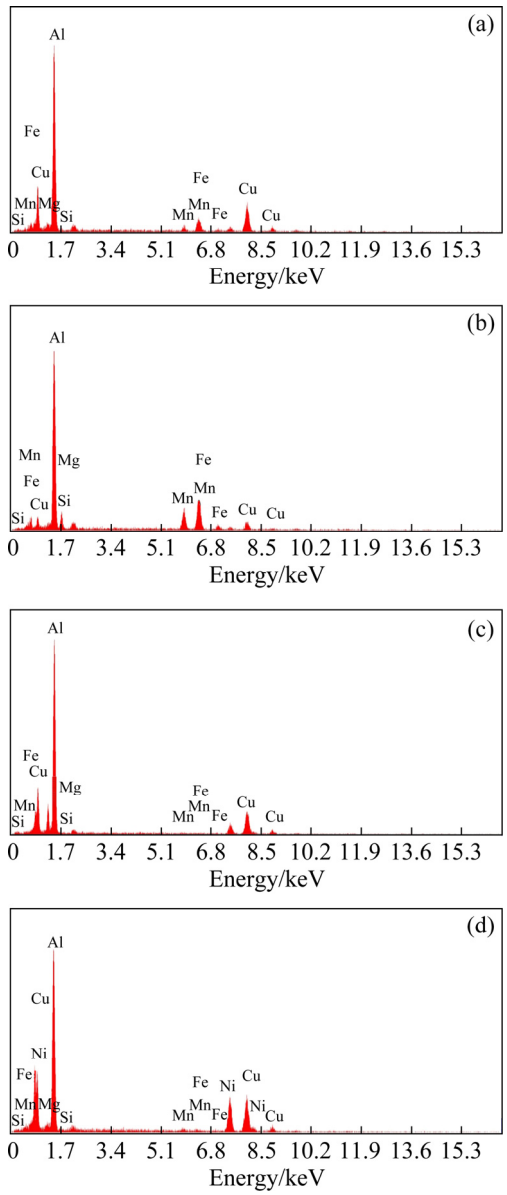

Fig. 5 EDS spectra of Al_7Cu_2Fe (Spot I) (a) Al(Cu,Mn,Fe,Si) (Spot II) (b), *S*-Al_2CuMg (Spot III) (c) and Al_3NiCu (Spot IV) (d) (Spots I−IV are represented in Fig. 4)

Table 1 EDS analysis results of Al_7Cu_2Fe (Spot I), Al(Cu,Mn,Fe,Si) (Spot II), *S*-Al_2CuMg (Spot III), and Al_3NiCu (Spot IV) in Fig. 4 (at.%)

Element	Spot I	Spot II	Spot III	Spot IV
Fe	10.71	7.32	0.73	0.87
Mg	0.55	0.43	14.71	0.91
Cu	19.23	2.34	15.34	24.19
Ni	–	–	–	25.41
Si	0.45	6.71	0.21	0.32
Mn	0.59	5.45	0.36	0.43
Al	68.47	77.75	68.65	47.87

are likely to be of *S* type. However, it should be noted that reducing the amount of soluble copper in the aluminum matrix reduces the driving force of precipitation, and this will reduce the amount and size of *S* precipitates in the aluminum matrix.

Figure 7 shows the DSC diagram of nickel-containing and nickel-free samples after solid solution heat treatment. The endothermic and exothermic peaks are named according to Ref. [26]. As shown in the DSC diagram, the following precipitation sequence can be considered for nickel-containing and nickel-free samples:

$$\alpha \rightarrow \text{GPB} \rightarrow S'' \rightarrow S' \rightarrow S\text{-}Al_2CuMg \quad (1)$$

According to the DSC diagram, the temperature range of *S*-Al_2CuMg precipitate formation is 240−340 °C. The SEM images related to this temperature range demonstrate that *S*-Al_2CuMg precipitates are formed inside aluminum grains in large quantities. However, the nickel-containing sample has fewer precipitates. The reduction in peak height associated with the DSC diagram can be linked to adding nickel reducing the precipitation ability, as evidenced by the reduction in the amount and size of *S* precipitates in the SEM images of the nickel-containing sample.

Figure 8 presents the aspect ratio and average size of nickel- and iron-rich compounds. As shown, the size of these compounds is not changed significantly after heat treatment, but their aspect ratio decreases. Since the dissolution temperature of these compounds is much higher than the solid solution temperature, no significant change is expected in the size of these particles. Nevertheless, due to their high aspect ratio before solid solution treatment, there is more driving force to reduce the specific surface area of these compounds. As a result, their aspect ratio is reduced during the solid solution treatment by absorbing soluble elements in the aluminum matrix.

3.2 Mechanical properties

Figure 9 shows the hardness changes of nickel-containing and nickel-free samples. As shown, the hardness increases with increasing temperature and then decreases. This trend of hardness changes is observed in both samples. However, the maximum hardness of the nickel-

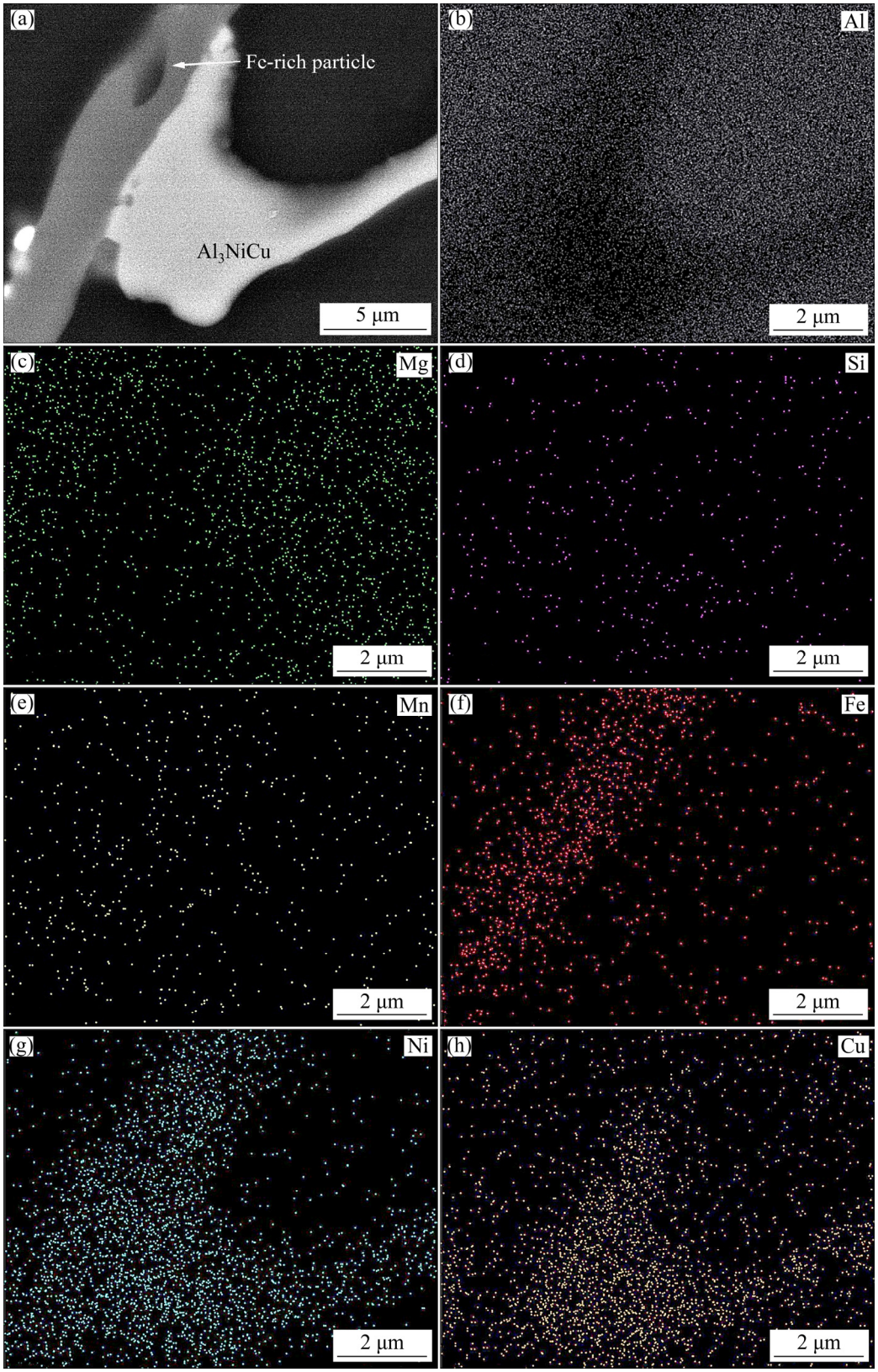

Fig. 6 SEM micrograph of Al_3NiCu and Fe-rich particles (a), and EDS mappings of elements (b−h)

containing sample is less than that of the nickel-free sample due to the adsorption of copper by nickel- and iron-rich compounds and the reduction of *S* precipitates. The results notably show lower hardness drop in the nickel-containing sample, while in general the hardness after solid solution

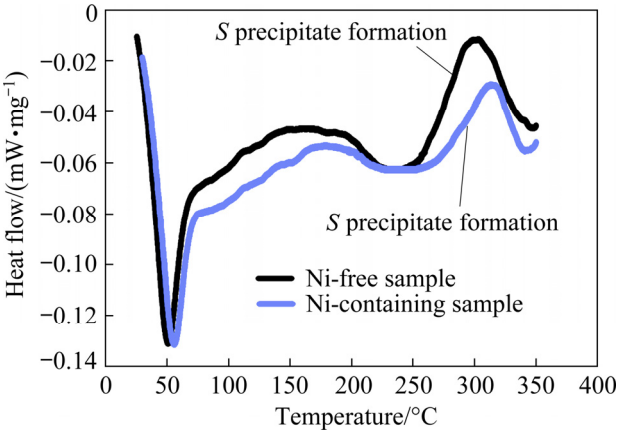

Fig. 7 DSC curves of nickel-free and nickel-containing samples

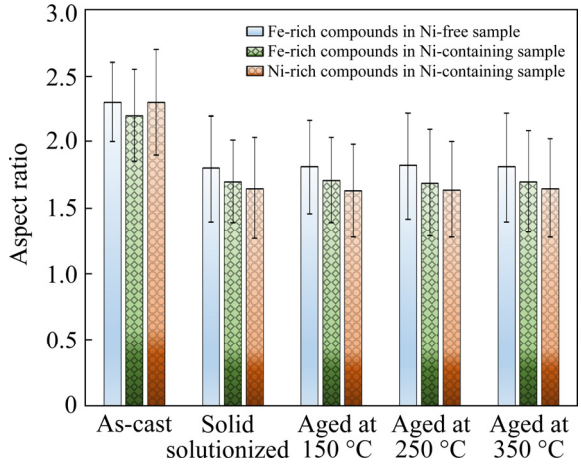

Fig. 8 Aspect ratio of Ni-rich and Fe-rich particles in microstructure of Ni-free and Ni-containing samples under different heat treatment conditions

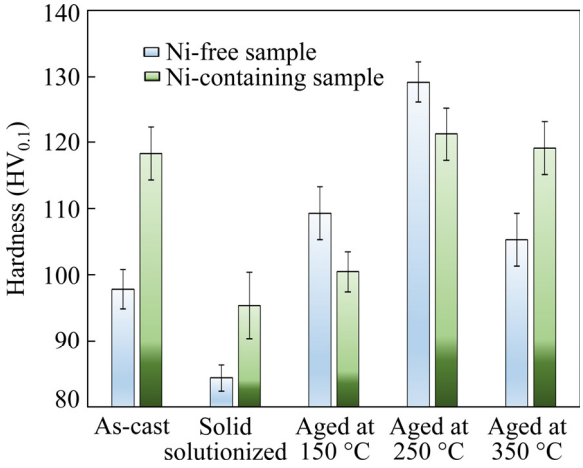

Fig. 9 Hardness of Ni-free and Ni-containing samples under different heat treatment conditions

treatment at the temperature of 350 °C is higher than that of the nickel-free sample. In other words, it can be said that adding nickel reduces the precipitation rate and the contribution of *S* precipitates in the strengthening of composite. The tensile test results of nickel-containing and nickel-free samples after non-isothermal aging treatment and after quenching in water are shown in Fig. 10. As shown, with the addition of nickel and aging treatment, the strength decreases to (221.67±8.31) MPa and the toughness increases to (1.67±0.08) MJ/m^3 compared to the nickel-free sample.

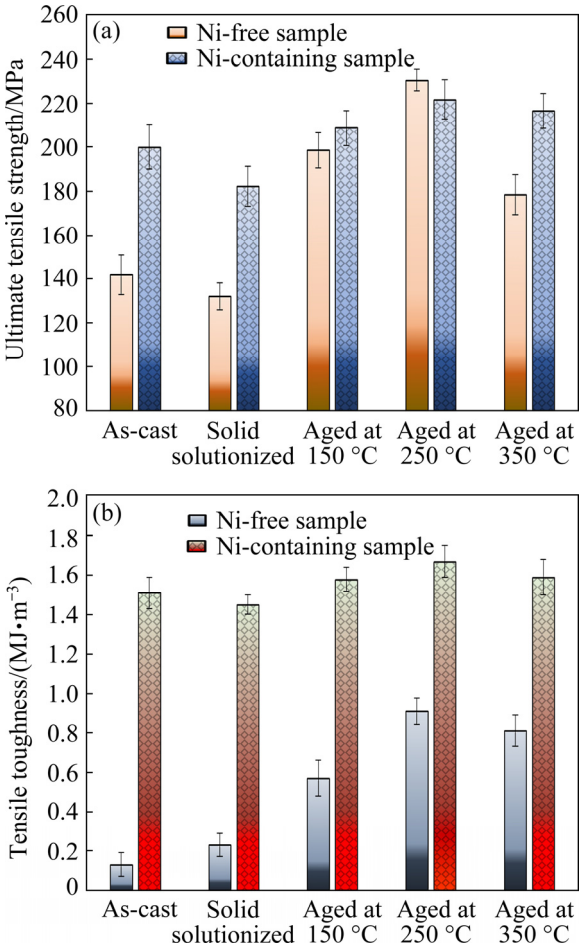

Fig. 10 Tensile strength (a) and toughness (b) of nickel-free and nickel-containing samples under different heat treatment conditions

Based on Refs. [27−29], the strength of the composite (σ_c) can be considered as a function of the matrix strength (σ_m), the volume fraction of reinforcing particles, and the aspect ratio of reinforcing particles. Considering the effect of porosity, the composite strength (σ_{cf}) can be calculated as

$$\sigma_{cf}=\sigma_c\exp(-KV_p) \quad (2)$$

where V_p is the porosity volume fraction, and K is a

constant. By considering the percentage of porosity in the nickel-containing and nickel-free samples, the more porosity in the nickel-containing sample can expectedly weaken the mechanical properties of the composite. In contrast, it should be noted that the presence of nickel-rich reinforcing phases due to the strong bond that it is formed with the aluminum matrix (according to microstructures) can act as a load-bearing component and thus help to increase the strength of the composite. However, it should be noted that according to micromechanics theories, various factors such as the strength induced by solid solution (σ_{SS}), grain size (σ_G), precipitates (σ_P), and modulus strengthening (σ_M) are effective in increasing the strength of the matrix. As the grain size of aluminum is (28.4±4.6) μm in the nickel-containing sample and (29.7±5.8) μm in nickel-free sample, the effect of this mechanism in strengthening can be avoided. Still, the contents of soluble copper in the aluminum matrix in both aged nickel-containing and nickel-free samples are 0.4 and 0.5 at.%, respectively. The SEM images show that in the nickel-free sample, most of the soluble copper is used to form *S* precipitates, and in the nickel-containing sample, soluble copper is used in the microstructure through the formation of *S* precipitates and adsorption to nickel-rich and iron-rich compounds. Therefore, the effect of strengthening through solid solution can be considered to be insignificant in both samples. The presence of reinforcing particles with different elastic moduli with the aluminum matrix can change the energy of the dislocations in the interface [30,31]. As the dislocations approach a phase with a different modulus, their energy changes, strengthening the composite. Since nickel-rich phases are not present in the nickel-free sample, there will be an additional strengthening mechanism in the nickel-containing sample. As previously mentioned in the microstructure section, the amount of *S* precipitates formed in the microstructure of the nickel-containing sample is much smaller than that of the nickel-free sample. As explained, the two strengthening mechanisms through precipitates and the strengthening mechanism through the module affect the strength changes of the nickel-containing and nickel-free samples. The lower maximum strength of the nickel-containing sample after non-isothermal aging at 250 °C compared to the nickel-free sample indicates that the effect of strengthening through precipitates is far greater than the strengthening through modulus difference.

Figure 11 shows the fracture surface of different samples. The brittle fracture nature is dominant in all samples. The cleavage fracture surfaces, microcracks, and shallow dimples can be seen in the fracture surfaces. After aging treatment, the amount of dimples on the fracture surface in nickel-containing and nickel-free samples decreases. As shown, particles with a significant aspect ratio act as stress concentration sites and are the source of microcrack formation in different samples. Since the dissolution temperature of these compounds is higher than the solid solution and aging treatment temperature, little change in the morphology of these compounds can be observed. Therefore, it can be seen that the nature of failure in different samples does not change significantly after heat treatment.

4 Conclusions

(1) The nickel-aluminide formation in the AA2024 aluminum alloy matrix has little effect on aluminum matrix grain size.

(2) Reducing the amount of soluble copper in the aluminum matrix reduces the driving force of precipitation during non-isothermal aging, reducing the amount and size of *S*-Al_2CuMg precipitates in the aluminum matrix.

(3) After homogenization and non-isothermal aging treatment, the size of nickel- and iron-rich compounds is not changed significantly; however, the aspect ratio of these compounds decreases.

(4) During the non-isothermal aging, the maximum hardness and ultimate tensile strength of AA2024−Al_3NiCu composite is 6% and 4%, respectively, less than those of the AA2024 without nickel-aluminide.

(5) The addition of nickel reduces the precipitation rate and the contribution of *S*-Al_2CuMg precipitates in the strengthening of composite.

(6) During non-isothermal aging treatment, the effect of strengthening through precipitates is far more significant than the modulus strengthening mechanism.

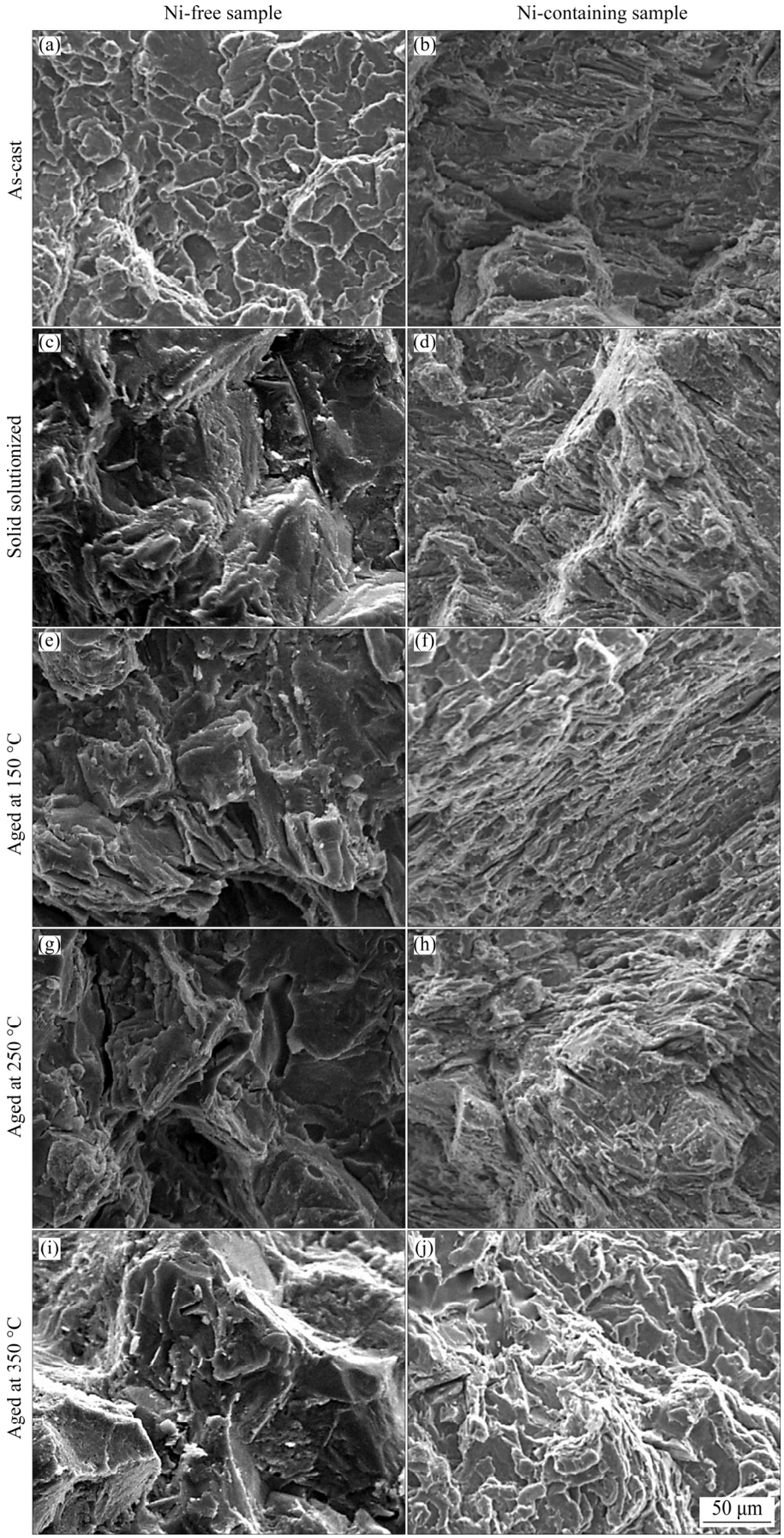

Fig. 11 SEM images of fracture surface of nickel-free and nickel-containing samples under different conditions

References

[1] GUPTA R, NANDA T, PANDEY O P. Comparison of wear behaviour of LM13 Al−Si alloy based composites reinforced with synthetic (B_4C) and natural (ilmenite) ceramic particles [J]. Transactions of Nonferrous Metals Society of China, 2021, 31(12): 3613−3625.

[2] NIE Q Q, CHEN G H, WANG B, YANG L, TANG W M. Process optimization, microstructures and mechanical/ thermal properties of Cu/Invar bi-metal matrix composites fabricated by spark plasma sintering [J]. Transactions of Nonferrous Metals Society of China, 2021, 31(10): 3050−3062.

[3] ZHOU Y, HE W J, MA J T, CHEN Z J, LIU Q. Annealing hardening and deformation behavior of layered gradient Zr−Ti composite [J]. Transactions of Nonferrous Metals Society of China, 2021, 31(8): 2358−2371.

[4] IMANIAN GHAZANLOU S, EGHBALI B, PETROV R. EBSD characterization of Al7075/graphene nanoplates/ carbon nanotubes composites processed through post-deformation annealing [J]. Transactions of Nonferrous Metals Society of China, 2021, 31(8): 2250−2263.

[5] VENCL A, BOBIC I, AROSTEGUI S, BOBIC B, MARINKOVIĆ A, BABIĆ M. Structural, mechanical and tribological properties of A356 aluminium alloy reinforced with Al_2O_3, SiC and SiC + graphite particles [J]. Journal of Alloys and Compounds, 2010, 506: 631−639.

[6] SALARIEH S, NOUROUZI S, JAMSHIDI AVAL H. An investigation on the microstructure and mechanical properties of Al−Zn−Mg−Cu/Ti composite produced by compocasting [J]. International Journal of Metalcasting, 2022, 16: 1397−1414. Doi: 10.1007/s40962-021-00698-1.

[7] RAJAK D K, PAGAR D D, KUMAR R, PRUNCU C I. Recent progress of reinforcement materials: A comprehensive overview of composite materials [J]. Journal of Materials Research and Technology, 2019, 8(6): 6354−6374.

[8] SHAYAN M, EGHBALI B, NIROUMAND B. Fabrication of AA2024−TiO_2 nanocomposites through stir casting process [J]. Transactions of Nonferrous Metals Society of China, 2020, 30(11): 2891−2903.

[9] KHAKI-DAVOUDI S, NOUROUZI S, JAMSHIDI AVAL H. Microstructure and mechanical properties of AA7075/Al_3Ni composites produced by compocasting [J]. Materials Today Communications, 2021, 28: 102537.

[10] MOHAMADIGANGARAJ J, NOUROUZI S, JAMSHIDI AVAL H. Microstructure, mechanical and tribological properties of A390/SiC composite produced by compocasting [J]. Transactions of Nonferrous Metals Society of China, 2019, 29(4): 710−721.

[11] LIU G, ZHAO N Q, SHI C S, LIU E Z, HE F, MA L Y, LI Q Y, LI J J, HE C N. In-situ synthesis of graphene decorated with nickel nanoparticles for fabricating reinforced 6061Al matrix composites [J]. Materials Science and Engineering A, 2017, 699: 185−193.

[12] BALAKRISHNAN M, DINAHARAN I, KALAISELVAN K, PALANIVEL R. Friction stir processing of Al_3Ni intermetallic particulate reinforced cast aluminum matrix composites: microstructure and tensile properties [J]. Journal of Materials Research and Technology, 2020, 9(3): 4356−4367.

[13] BOTELHO T M, AZEVEDO H M, MACHADO G H, BARBOSA C R, ROCHA F S, COSTA T A, ROCHA O L. Effect of solidification process parameters on dry sliding wear behavior of AlNiBi alloy [J]. Transactions of Nonferrous Metals Society of China, 2020, 30(3): 582−594.

[14] ARUL S. Effect of nickel reinforcement on micro hardness and wear resistance of aluminium alloy Al7075 [J]. Materials Today: Proceedings, 2020, 24: 1042−1051.

[15] VISHWANATHA A, PANDA B, SHIVANNA D. Effect of a T6 aging treatment on the corrosion behaviour of in-situ Al_xNi_y reinforced AA6061 composite [J]. Materials Today: Proceedings, 2021, 44: 4112−4117.

[16] ABUTHAKIR J, SUBRAMANIAN R, KAVITHA M, VENKATESH G, MANIKANDAN P. Corrosion studies of Al_x−Ni in-situ intermetallics reinforced Al metal matrix composites [J]. Materials Today: Proceedings, 2020, 28: 1158−1163.

[17] RAMESH R, SURESH KUMAR S, GOWRISHANKAR S, Production and characterization of aluminium metal matrix composite reinforced with Al_3Ni by stir and squeeze casting [C]//Applied Mechanics and Materials. Trans Tech Publ, 2015: 315−319.

[18] MATSUMURO M, KITSUDO T. Fabrication of in-situ intermetallic compound dispersed aluminum matrix composites by addition of metal powders [J]. Materials Transactions, 2006, 47(12): 2972−2979.

[19] FARAJOLLAHI R, JAMSHIDI AVAL H, JAMAATI R. Effects of Ni on the microstructure, mechanical and tribological properties of AA2024-Al_3NiCu composite fabricated by stir casting process [J]. Journal of Alloys and Compounds, 2021, 887: 161433.

[20] ASM HANDBOOK. Heat Treating [M]. Vol. 4. ASM International, Materials Park, OH, 1991.

[21] TAYLOR R, MCCLAIN S, BERRY J. Uncertainty analysis of metal-casting porosity measurements using Archimedes' principle [J]. International Journal of Cast Metals Research, 1999, 11(4): 247−257.

[22] LIN Y, XIA Y C, JIANG Y Q, LI L T. Precipitation in Al−Cu−Mg alloy during creep exposure [J]. Materials Science and Engineering A, 2012, 556: 796−800.

[23] LI S, ZHANG J, YANG J, DENG Y, ZHANG X. Influence of Mg contents on aging precipitation behavior of Al−3.5Cu−xMg alloy [J]. Acta Metallurgica Sinica (English Letters), 2014, 27(1): 107−114.

[24] BARROS A, da CRUZ C B, SILVA A P, CHEUNG N, GARCIA A, ROCHA O L, MOREIRA A L S. Length scale of solidification microstructure tailoring corrosion resistance and microhardness in T6 heat treatment of an Al−Cu−Mg alloy [J]. Corrosion Engineering, Science and Technology, 2020, 55(6): 471−479.

[25] GARCÍA-HERNÁNDEZ J L, GARAY-REYES C G, GÓMEZ-BARRAZA I K, RUIZ-ESPARZA-RODRÍGUEZ M A, GUTIÉRREZ-CASTAÑEDA E J, ESTRADA-GUEL I, MALDONADO-OROZCO M C, MARTÍNZ-SÁNCHEZ R. Influence of plastic deformation and Cu/Mg ratio on the

strengthening mechanisms and precipitation behavior of AA2024 aluminum alloys [J]. Journal of Materials Research and Technology, 2019, 8(6): 5471−5475.

[26] WANG S C, STARINK M J. Two types of *S* phase precipitates in Al−Cu−Mg alloys [J]. Acta Materialia, 2007, 55(3): 933−941.

[27] LEE I, HSU C, CHEN C, HO N, KAO P. Particle-reinforced aluminum matrix composites produced from powder mixtures via friction stir processing [J]. Composites Science and Technology, 2011, 71(5): 693−698.

[28] HONG S H, CHUNG K H, LEE C H. Effects of hot extrusion parameters on the tensile properties and microstructures of SiC_w−2124Al composites [J]. Materials Science and Engineering A, 1996, 206: 225−232.

[29] NARDONE V, PREWO K. On the strength of discontinuous silicon carbide reinforced aluminum composites [J]. Scripta Metallurgica, 1986, 20: 43−48.

[30] PANDEY P, MAKINENI S K, GAULT B, CHATTOPADHYAY K. On the origin of a remarkable increase in the strength and stability of an Al rich Al−Ni eutectic alloy by Zr addition [J]. Acta Materialia, 2019, 170: 205−217.

[31] DIXIT M, MISHRA R S, SANKARAN K K. Structure–property correlations in Al 7050 and Al 7055 high-strength aluminum alloys [J]. Materials Science and Engineering A, 2008, 478: 163−172.

原位 AA2024−Al_3NiCu 复合材料的非等温时效行为

Ramezanali FARAJOLLAHI, Hamed JAMSHIDI AVAL, Roohollah JAMAATI

Department of Materials Engineering, Babol Noshirvani University of Technology,
Shariati Avenue, Babol 47148-71167, Iran

摘　要：研究非等温时效处理对搅拌铸造原位 AA2024−Al_3NiCu 复合材料显微组织和力学性能的影响。在搅拌铸造过程中加入 3%(质量分数)的镍粉，铸造后在 500 ℃均匀化热处理 24 h，得到 Al_3NiCu 金属间化合物。光学显微镜和扫描电镜观察结果表明，经非等温时效处理后，*S*-Al_2CuMg 析出相得到细化，在枝晶之间形成该析出相的贫相区。在搅拌铸造过程中添加镍，降低 *S*-Al_2CuMg 析出相的析出速率及其在非等温时效处理过程中对复合材料的强化作用。含 3%镍的样品在 250 ℃非等温时效处理后可获得最大的硬度、极限抗拉强度和韧性，分别为：(121.30±4.21) HV, (221.67±8.31) MPa 和(1.67±0.08) MJ/m^3。与不含镍的 AA2024 铝合金相比，AA2024−Al_3NiCu 复合材料的最大硬度和极限抗拉强度分别降低 6%和 4%。

关键词：AA2024 基复合材料；搅拌铸造法；非等温时效处理；Al_3NiCu 增强相

(Edited by Bing YANG)